Selective observation of local carrier dynamics at step bunches on vicinal TiO_2 (110) by time-resolved pump-probe second harmonic generation method

Hiroaki Takahashi, Yoshihiro Miyauchi, and Goro Mizutani*

School of Materials Science, Japan Advanced Institute of Science and Technology, Asahidai, Nomi, Ishikawa 923-1292, Japan

(Received 11 August 2011; published 26 July 2012)

We report on a step-selective time-resolved second harmonic generation (SHG) method using vicinal TiO_2 (110) with regularly aligned step bunches. The step selectivity was realized by taking advantage of the symmetry-selective properties of second order nonlinear optical processes. In the time-resolved pump-probe SHG measurement, the step bunches displayed a unique temporal response or a sharp spike decaying within ~100 ps, while no decay kinetics was observed for the (110) terraces within a nanosecond. The observed unique local dynamics at the step bunches was attributed to a transient change in their local carrier density. This carrier density change at the step bunches was discussed from the aspect of their local density of states (LDOS) by using step-selective second harmonic and sum frequency generation (SHG/SFG) spectroscopy and density functional theory (DFT) calculation.

DOI: 10.1103/PhysRevB.86.045447 PACS number(s): 73.20.At

I. INTRODUCTION

TiO_2 is a well-known photocatalyst, and the mechanism of its photocatalytic reactions has been intensively studied since the discovery of the Honda-Fujishima effect.[1–5] Surface defect study of TiO_2 has attracted much attention because defects such as steps,[6–11] kinks, surface oxygen vacancies,[12–23] and near-surface titanium interstitials[24–26] are known to have a strong influence on molecular adsorption and photocatalytic reactions as catalytic active sites. Especially, much effort has been devoted to studying surface oxygen vacancies, and their electronic properties have been revealed over the last few decades.[12–23] In contrast, the electronic properties of steps and kinks have not been experimentally understood yet due to the difficulty in selectively analyzing their weak signals as well as controlling their area density.

Optical second harmonic generation (SHG) is a potential tool to analyze step structures, and its high sensitivity to steps has been suggested for decades.[28–32] SHG is a second order nonlinear optical process and is allowed only in media without inversion symmetry under the electric dipole approximation. By choosing a proper vicinal surface of a centrosymmetric single crystal such as TiO_2 (110), it is basically feasible to selectively extract the electronic information of regularly aligned steps.[29,32–35]

For vicinal TiO_2 (110), the step selectivity of SHG can be described phenomenologically as below. When the electric fields of fundamental and reflected SHG light are set almost parallel to the terrace plane of vicinal TiO_2 (110), surface SHG from the (110) terraces is forbidden since the C_{2v} symmetry of the (110) plane does not have broken symmetry in the direction parallel to the terrace. On the other hand, the step sites give rise to broken symmetry in the step face direction. Thus electrons only at the step sites feel asymmetric potential during their forced oscillation and then cause SHG radiation. This scenario is approximately realized by using the optical geometry of either normal incidence or S in–S out polarization geometry. We refer to this optical geometry as a step-selective configuration in this paper. It is valid only when quadrupole bulk SHG is assumed to be negligible with respect to the dipole surface SHG from the step sites on vicinal TiO_2 (110). We paid attention to this point in this paper as well.

The step selectivity of the above SHG measurement depends especially on the symmetry of the terrace parts on the vicinal surface. For instance, when terraces have C_{3v} or C_s symmetry, surface SHG from the terraces is generally allowed even under the step-selective configuration, and resultantly it is often difficult to extract pure step contribution from the mixture of the two contributions. C_{3v} symmetric terraces are characteristic to the ideal (111) planes of fcc and bcc lattices and the (0001) plane of a hcp lattice. These are the cases with most of the SHG studies involving vicinal surfaces.[28,30,31,36–38] On the other hand, terraces with C_{2v} or C_{4v} symmetry, such as TiO_2 (110) and Si (110), do not allow SHG radiation in the above optical geometry, and this condition provides surface SHG with the step-selective property. However, the number of research groups handling the latter case is limited.[29,32–35] The first selective detection of the pure step contribution through SHG was done by Rasing and his co-workers for vicinal Si (110) under S in–S out polarization geometry.[32] In spite of the great potential of this discovery, it has not triggered much attention to further application of this SHG property as a new surface analytical method. We have casted new light on this issue and have developed the surface probe experimentally analyzing local density of states (LDOS) at step sites using vicinal TiO_2 (110) by incorporating the step-selective scheme into SHG spectroscopy.[33,34]

In our previous report, we discussed a difference in electronic properties between (110) terraces and step bunches formed on TiO_2 (15 15 4) in terms of the LDOS distribution near the band-gap regions by using the above-mentioned method.[34] The result indicated that the density of states of the valence and/or conduction bands for the step bunches is distributed energetically closer to the gap regions than that for the (110) terraces. We suggested that this difference can perturb carrier dynamics in the vicinity of the step bunches and may result in different reactivity between the steps and terraces on TiO_2 (15 15 4). This is interesting from the aspect of the electronic role of steps in photocatalytic reactions. However, it is technically very difficult to investigate fast carrier dynamics at

step sites directly, and no relevant technique has been reported except that relatively slow molecular dynamics of adsorption and desorption at step sites was traced by scanning tunneling microscopy (STM).[10,11] In this report we demonstrate selective measurement of fast local dynamics at the step bunches on TiO_2 (15 15 4) by utilizing the step-selective SHG.

Time-resolved pump-probe techniques using optical SHG or sum frequency generation (SFG) have been widely used as powerful tools to investigate dynamics at surfaces or interfaces.[39–48] For instance, Domen *et al.* found heat-driven migration of the formate adsorbed on a TiO_2 surface between different surface active sites using time-resolved pump-probe vibrational SFG spectroscopy.[39] Lantz *et al.* carried out time-resolved SHG spectroscopy for an *n*-doped single crystal TiO_2 (001) electrode and observed that electric-field-induced second harmonic generation (EFISHG) from a space charge layer of the TiO_2 electrode was quenched transiently by the migration of photoexcited holes to the TiO_2 surface.[40]

In this study we combined the above pump-probe technique with the step-selective SHG in order to selectively observe local dynamics at the step bunches of TiO_2 (15 15 4). A detailed discussion on the step selectivity of SHG will be given in the Appendix. Before moving on to the time-resolved SHG measurement, we inspected the local density of states at the step bunches by using SHG and electronic SFG spectroscopy (SHG/SFG spectroscopy) in the step-selective configuration[33] and density functional theory (DFT) calculation. Taking the result of this LDOS analysis into account, local dynamics at the step bunches was discussed through the time-resolved pump-probe SHG measurement.

II. EXPERIMENT

We purchased single crystal rutile TiO_2 plates with optically flat (15 15 4) faces from K&R creation Co., Ltd. The (15 15 4) plane is a vicinal surface of (110) off-oriented toward the [001] direction by 16.2 deg. Before being delivered, the samples had been polished by diamond abrasive grains with the sizes of 5, 2, and 0.5 μm in series, and then had been treated by mechanochemical processing. We prepared two types of TiO_2 (15 15 4) surfaces. One is exactly the same sample as was used in our earlier study.[34] This was prepared by annealing of the as-delivered sample at 800 °C in an O_2 gas for 2 h. Before and after the annealing, the sample went through chemical etching by a 5% HF aqueous solution. The other sample was prepared just by HF etching of the as-received wafer. The former and the latter are referred to as the annealed and unannealed samples in this paper, respectively. We employed the unannealed sample as a reference sample in order to compare the properties between surfaces with and without step bunching.

In this paper we performed noncontact atomic force microscopy (NC-AFM), SHG/SFG spectroscopy, and time-resolved pump-probe SHG measurement. All the measurements were carried out in an ambient condition.

The experimental setups for the SHG spectroscopy and the electronic SFG spectroscopy[33] are shown in Figs. 1(a) and 1(b), respectively. The light source for the SHG spectroscopy

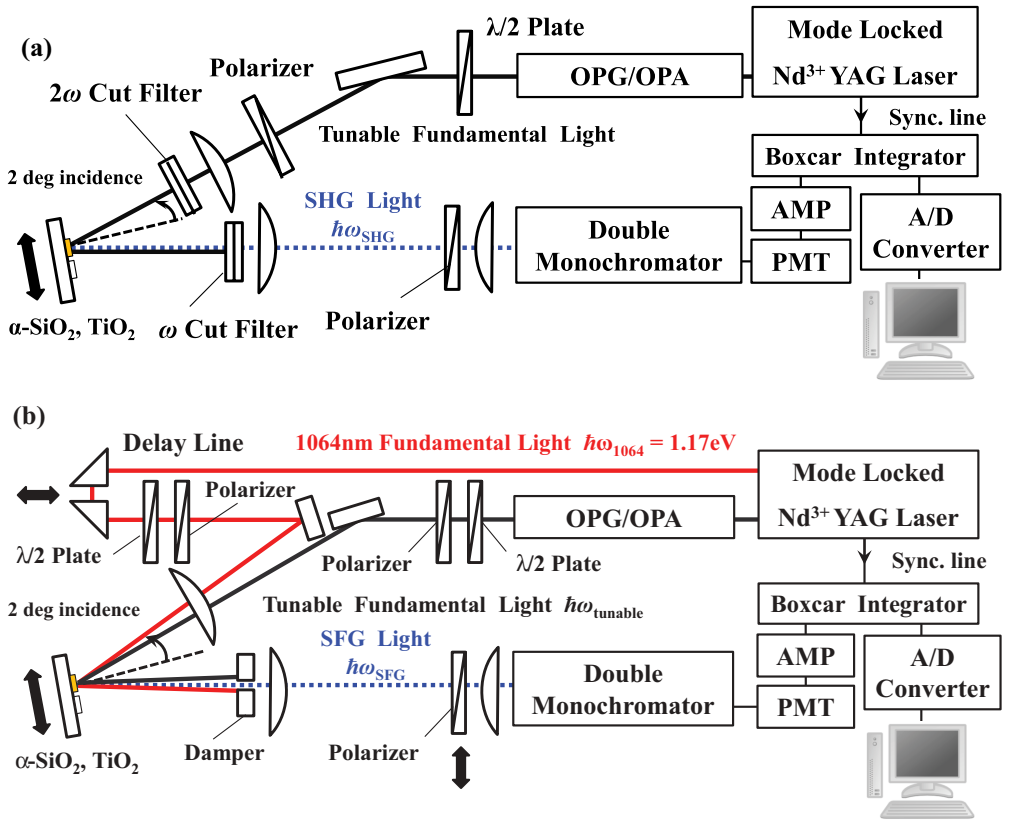

FIG. 1. (Color online) Experimental setups for (a) the SHG spectroscopy and (b) the electronic SFG spectroscopy. PMT and AMP represent a photomultiplier and an amplifier, respectively.

was delivered by an optical parametric generator and amplifier (OPG/OPA) system driven by a frequency-tripled mode-locked Nd^{3+}:YAG laser (355 nm) running at a repetition rate of 10 Hz and at a pulse width of 30 ps. In the SHG spectroscopy, SHG photon energy $\hbar\omega_{SHG}$ was varied from 2.35 to 3.35 eV and from 3.65 to 4.65 eV by the OPG/OPA system. SHG data at the photon energies between 3.35 and 3.65 eV are unavailable due to the property of the OPG/OPA system. The electronic SFG spectroscopy was employed to compensate for this photon energy range and to detect one-photon resonances. In the electronic SFG spectroscopy, two incident beams were obtained from the OPG/OPA system and the fundamental light of the mode-locked Nd^{3+}:YAG laser (1064 nm). The SFG photon energy $\hbar\omega_{SFG} = \hbar\omega_{tunable} + \hbar\omega_{1064}$ was tuned from 2.59 to 2.84 eV and from 3.00 to 3.90 eV. $\hbar\omega_{tunable}$ and $\hbar\omega_{1064}$(=1.17 eV) denote the photon energies of two fundamental beams. The incident angles of the excitation beams from the OPG/OPA system were fixed at ~2 deg in the SHG/SFG spectroscopy, and the fundamental 1064 nm beam in the electronic SFG spectroscopy was incident at ~4 deg, so that the fundamental and reflected SHG electric fields were nearly parallel to the terrace plane of annealed TiO_2 (15 15 4) (step-selective configuration). The incident planes were set parallel to $[1\bar{1}0]$, or the step edge direction. The polarization combination of fundamental and reflected SHG/SFG beams were set at S in–S out or P in–S out. In the SFG measurement, the polarizations of the two incident beams were always kept the same. The SHG/SFG intensity was calibrated by the signals from α-SiO_2 (0001) since the optical system itself has sensitivity variations with respect to the SHG/SFG photon energy.

The experimental setup for the time-resolved pump-probe SHG measurement is shown in Fig. 2. A 355 nm UV pump light (photon energy 3.49 eV) was obtained from the third harmonic generation (THG) of the fundamental light of the mode-locked Nd:YAG laser used in the SHG/SFG spectroscopy. The spot size of the pump light was about 4 mm on the sample surfaces, and its average power density was varied up to ~8 mW/cm^2. The corresponding maximum fluence was about 0.8 mJ/cm^2. The electronic response at the (110) terraces or step sites was probed by monitoring SHG from the pumped (15 15 4) surface at the photon energy of 4.66 eV. The 532 nm fundamental light (photon energy 2.33 eV) for the SHG was delivered by the frequency-doubled mode-locked Nd:YAG laser. The spot size of the probe light was about 1 mm, and its fluence was about 7–13 mJ/cm^2. Even though the probe fluence was about ten times as large as the pump fluence, a self-action by the probe light is negligible mainly because its photon energy of 2.33 eV is less than the band gap of rutile TiO_2, 3.06 eV. In fact, SHG intensity showed quadratic dependence as a function of the incident probe fluence. The incident angle of the probe light was fixed at ~45 deg. The step-selective SHG measurement for annealed TiO_2 (15 15 4) was carried out under the S in–S out polarization geometry with the $[1\bar{1}0]$ azimuth. This optical configuration allows the input and output electric fields to be nearly parallel to the terrace plane and to cross the step edges. We also observed SHG with the P in–all out polarization geometry in order to roughly compare SHG temporal responses between the step bunches and (110) terraces on the annealed surface. Note that "all" in the notation of P in–all out denotes both S and P polarizations. For P in–all out, the incident plane was set parallel to [001], or perpendicular to the step edges, and the incident probe light was delivered in the direction to descend the steps. While the step contribution under this optical configuration may get relatively large for annealed TiO_2 (15 15 4), the terrace contribution contained in the SHG signals becomes even larger for the 45 deg incidence especially when the targeted photon energy range is above ~4 eV, as will be mentioned in Sec. III C.

Calculation of local density of states at step sites on vicinal TiO_2 (110) was performed within the framework of DFT to support the analysis by the SHG/SFG spectroscopy. The DFT calculation was carried out under the generalized-gradient approximation (GGA) with the Perdew-Burke-Ernzerhof (PBE) exchange-correlation functional[49] using the CASTEP code[50] as implemented in the Materials Studio 5.5 software package (Accelrys Software, Inc.). Wave functions were expanded in plane waves with a cutoff energy of 340 eV, and ultrasoft pseudopotentials were used to describe Ti and O atoms. The calculated model has a (4 4 1) plane, and the surface consists of a (110) terrace and a bilayer step with a (111) step face as will be shown later in Fig. 6(a). The bilayer step is the simplest model for the multilayer step bunching observed on annealed TiO_2 (15 15 4) in Sec. III A.

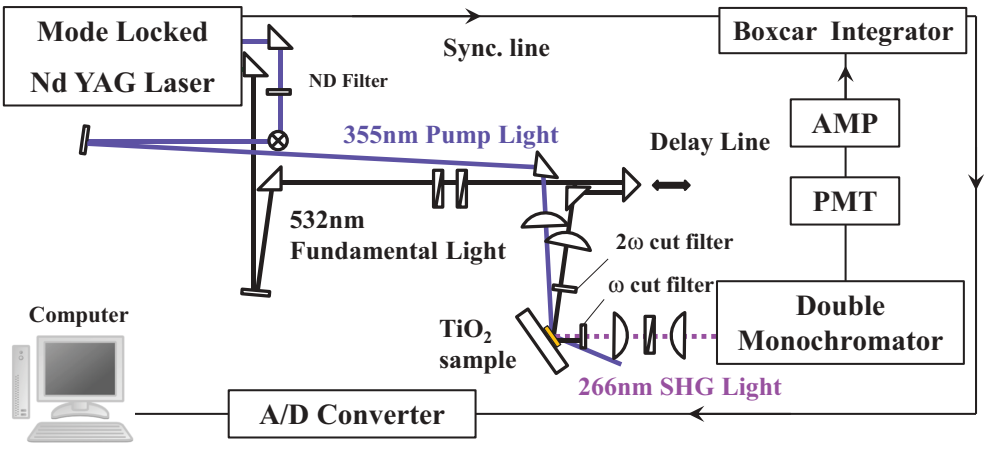

FIG. 2. (Color online) Experimental setup for the time-resolved pump-probe SHG measurement.

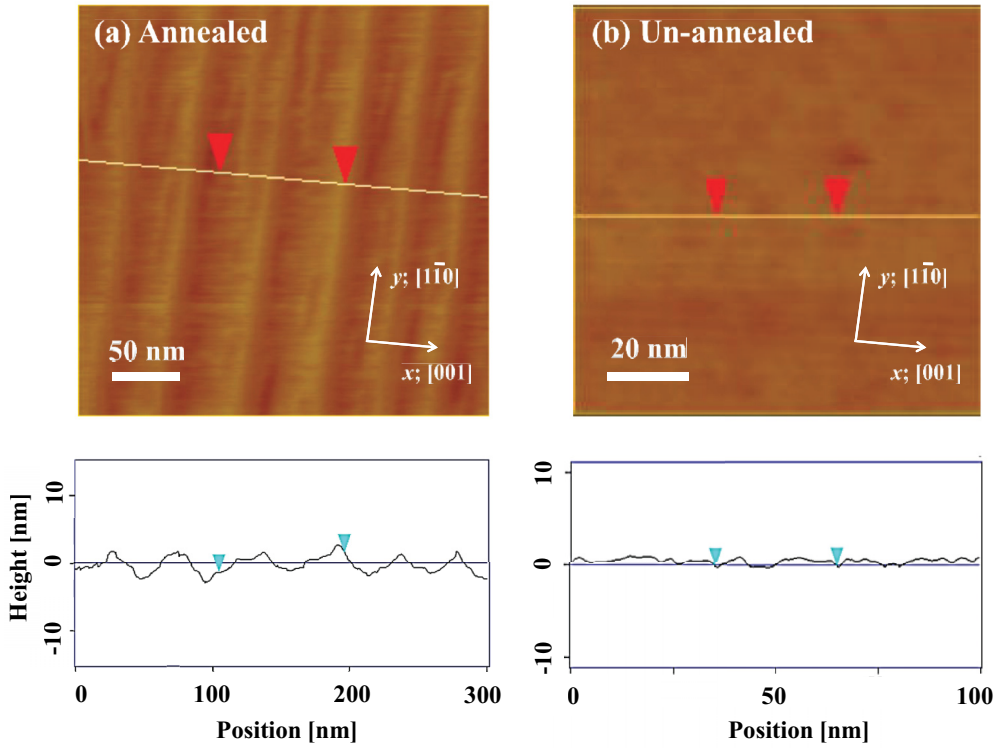

FIG. 3. (Color online) Topography images and height profiles of (a) annealed TiO_2 (15 15 4) and (b) unannealed TiO_2 (15 15 4) measured by NC-AFM.

III. RESULTS AND DISCUSSION

A. Morphology of annealed and unannealed TiO_2 (15 15 4)

Topography images of the annealed and unannealed TiO_2 (15 15 4) surfaces obtained by NC-AFM are shown in Fig. 3. As already reported in our earlier work,[35] the annealed sample surface is made up of multilayer step bunches (>10 ML) and flat (110) terraces [Fig. 3(a)]. The average interval between the step bunches is about 40 nm. The surface morphology of the annealed sample is schematically drawn in Fig. 4(a).

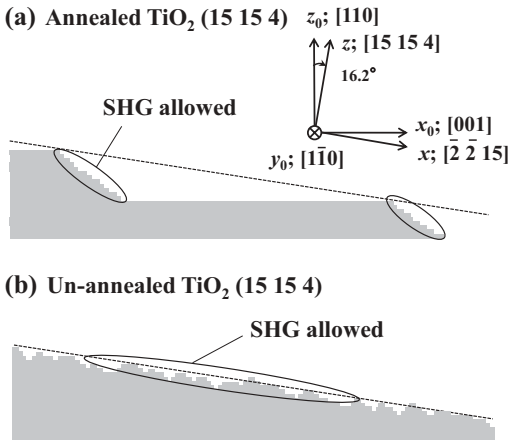

FIG. 4. Schematic surface structures of annealed and unannealed TiO_2 (15 15 4), and origins of SHG (or SFG) from their surfaces under the optical configuration of the S in–S out polarization combination or normal incidence.

In the image of the unannealed sample in Fig. 3(b), no clear step structure separated by wide (110) terraces was observed. The unannealed surface has a roughness of amplitude less than a nanometer and is actually flatter than the faceted annealed surface. To interpret this surface we assume that the surface consists of very fine but rather disordered steps and (110) terraces separated probably in the length scale of several angstroms with some surface defects, although they cannot be strictly defined as steps and terraces. As depicted in Fig. 4(b), for instance, the average number of these steps going downwards is larger than that of the steps going upwards, and this gives rise to asymmetry in the horizontal direction (x direction) on the unannealed surface.

B. Near-gap local density of states of the step bunches on annealed TiO_2 (15 15 4)

In this section we show the results of the SHG/SFG spectroscopy and the DFT calculation, and analyze the local density of states of the step bunches experimentally and theoretically to assist the discussion on local dynamics at the step bunches given in the next section. The SHG spectra of annealed and unannealed TiO_2 (15 15 4) are shown in Figs. 5(a) and 5(c). The corresponding electronic SFG spectra are shown in Figs. 5(b) and 5(d). The SHG/SFG spectra in Figs. 5(a) and 5(b) are relevant to $|\chi_{xyy}|^2$, and those in Figs. 5(c) and 5(d) are relevant to $|\chi_{xxx}|^2$. Here χ_{ijk} is a second order nonlinear susceptibility element in the $\{x, y, z\}$ coordinate system (Fig. 4). The SHG spectra of the annealed sample in Figs. 5(a) and 5(c) are identical to the ones shown in Ref. 34, except for the scanning photon energy range. In Figs. 5(c)

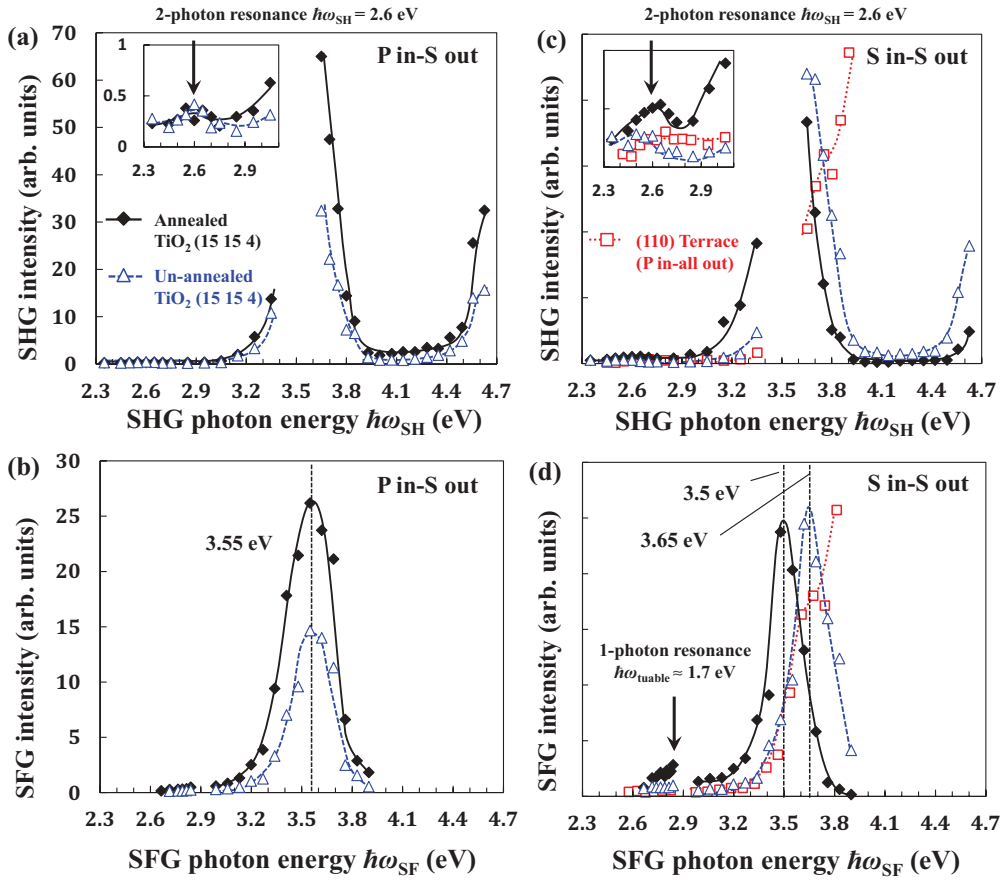

FIG. 5. (Color online) SHG/SFG spectra of annealed and unannealed TiO_2 (15 15 4). (a) SHG spectra for P in–S out, (b) SFG spectra for P in–S out, (c) SHG spectra for S in–S out, and (d) SFG spectra for S in–S out. In (c) and (d), SHG/SFG spectra of TiO_2 (110)[33] are also shown for comparison (dotted curve and empty squares). The scale of the vertical axis for each spectrum in (c) and (d) is not equivalent. The curves are guidelines.

and 5(d) the SHG/SFG spectra of TiO_2 (110) obtained in our recent work[33] are also shown as a dotted curve in order to highlight the difference in the SHG/SFG response energy between the step bunches and terraces.

We first consider the higher order electromagnetic response from bulk under the step-selective configuration because it can be generally as large as the targeted signal of dipole surface SHG from the step bunches on TiO_2 (15 15 4). Our previous rotational SHG measurement for TiO_2 (110) at the SHG photon energy of 4.66 eV showed that quadrupole bulk SHG from the (110) face is almost at the noise level for the nearly normal incidence.[35] Analogously, the corresponding bulk contribution from the vicinal (110) face in question is expected to be as small. In fact, the clearly different SFG responses between annealed and unannealed TiO_2 (15 15 4) in Fig. 5(d) ensure that the primary SHG/SFG resonances around 3.5 eV in Fig. 5 are ascribed to the surface dipole contribution from their different surface structures, not to bulk contribution. If the higher order effect from bulk were dominant in these two samples, they would have shown almost the same SHG/SFG responses since the annealed and unannealed samples have almost the same bulk properties. It is also worthwhile to mention here that these two samples display quite different azimuthal angle dependences of SHG intensity at the SHG photon energy of 4.66 eV (see Supplemental Material, Fig. S1[51]). The obtained rotational SHG patterns were almost perfectly fitted with the phenomenologically calculated curves under the electric dipole approximation. These facts suggest that the surface dipole contribution is predominant on TiO_2 (15 15 4) at least around the main resonant energies of ~3.5 and ~4.6 eV.

For the nearly normal incidence, surface SHG/SFG from annealed TiO_2 (15 15 4) shows step selectivity as illustrated in Fig. 4(a) (see Appendix for details). Thus its SHG/SFG spectra in Fig. 5 reflect the local electronic structure of the step bunches. On the other hand, surface SHG/SFG from unannealed TiO_2 (15 15 4) does not show step selectivity since the surface has no distinct step structure separated by a wide (110) terrace [Fig. 4(b)]. As explained in Sec. III A, the unannealed surface possesses asymmetry in the x direction (C_s symmetry), and this asymmetry drives SHG/SFG from the entire surface for the nearly normal incidence.

In Fig. 5 clear spectral differences are seen between the annealed and unannealed samples. As one of the interpretations, an incoherent diffuse SHG process, so-called hyper Rayleigh scattering (HRS),[52–54] may contribute to such spectral differences due to the disordered surface structure of unannealed TiO_2 (15 15 4). However, we judge that the spectral

differences are indeed due to their different local electronic properties. As our experimental and theoretical analysis of second order nonlinear susceptibility found out (Fig. S1),[51] χ_{xyy} governs the SHG processes at 4.66 eV rather than χ_{xxx} for the annealed surface, whereas it is the other way around for the unannealed surface. This difference in the proportions between χ_{xyy} and χ_{xxx} suggests that there is a remarkable difference in spatial distribution of wave functions between the annealed and unannealed surfaces. Such different local electronic properties between annealed and unannealed TiO_2 (15 15 4) lead to different spectral behaviors of χ, and result in different SHG/SFG responses as are seen in Fig. 5. The peak shift seen in Fig. 5(d) is one of the examples showing this effect.

In contrast to the case of S in–S out in Fig. 5(d), there is no particular difference in the main peak positions between the annealed and unannealed samples for P in–S out in Fig. 5(b). This result suggests that the χ_{xxx} component is more sensitive to the differences in microscopic surface structures and their electronic properties than the χ_{xyy} component. In the following discussion on the local electronic structure of the step bunches, we especially focus on the case of the S in–S out polarization geometry in Figs. 5(c) and 5(d).

The SFG peak of annealed TiO_2 (15 15 4) centered at 3.5 eV in Fig. 5(d) is assigned to the two-photon resonances of valence-conduction interband electronic transitions at the step bunches. Since this SHG/SFG response rises above ~3.1 eV (cf. 3.06 eV for the direct band gap of rutile TiO_2) and almost disappears above ~4.0 eV, the LDOS of the valence and conduction bands formed by the step bunch atoms must be mainly distributed within the range of ~4.0 eV across the band gap as shown in Fig. 7(a). Another rise in SHG intensity above ~4.5 eV in Fig. 5(c) implies the presence of another energy band ~1.4 eV below the valence band maximum (VBM) or above the conduction band minimum (CBM). The former case is illustrated in Fig. 7(a).

In Fig. 5(d) one can readily see that the SFG spectrum of the step bunches (solid curve) exhibits lower energy responses than that of the (110) terraces (dotted curve). This can be well explained from the result of the DFT calculation in Fig. 6. The model of the (4 4 1) surface for the DFT calculation is shown in Fig. 6(a). Partial density of states (PDOS) was calculated for several atoms located in bulk, on a (110) terrace, and at a step as shown in Figs. 6(b)–6(e). Since the calculated surface in Fig. 6(a) does not exactly model the actual surface structure of annealed TiO_2 (15 15 4) with multilayer step bunching, the DFT calculation cannot be used to directly analyze the detailed band structure of the step bunches but gives us an idea of relative differences in PDOS among different atomic structures. In Figs. 6(b) and 6(d) the valence band PDOS of the O atoms at the step site *S*-O1 and *S*-O2 is markedly blue shifted with respect to that at the terrace site *T*-O1 and *T*-O2. In contrast, no significant difference between the step and terrace sites was observed in the conduction band PDOS of Ti atoms. Therefore, the lower SHG/SFG energy responses of the step bunches can be attributed to the blue shift of their valence band PDOS. This difference in PDOS is illustrated in Fig. 7(a).

In the spectra of annealed TiO_2 (15 15 4), small SHG/SFG enhancements are seen at the SHG/SFG photon energies of 2.6 eV in Figs. 5(a) and 5(c), and at ~2.85 eV in Fig. 5(d). The SFG enhancement at ~2.85 eV is a one-photon

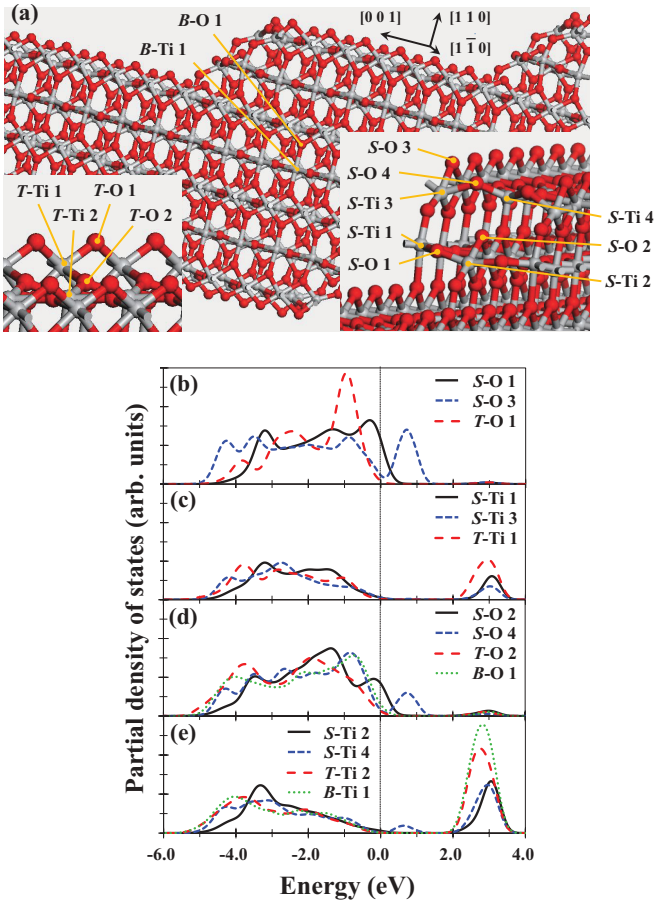

FIG. 6. (Color online) (a) A model of TiO_2 (4 4 1) used in the DFT calculation. (b) PDOS of the O atoms at the step and terrace sites along a bridging oxygen chain. (c) PDOS of the Ti atoms at the step and terrace sites along a bridging oxygen chain. (d) PDOS of the O atoms at the step and terrace sites along a titanium trough (fivefold Ti) and the one in the bulk. (e) PDOS of the Ti atoms at the step and terrace sites along a titanium trough (fivefold Ti) and the one in the bulk. In (a), double the size of the actual model is shown to recognize the structure with ease. The insets are the magnified views of the terrace and step sites. *B*, *T*, and *S* in the notations such as *B*-Ti1, *T*-O2, and *S*-O3 indicate bulk, terrace, and step, respectively.

resonance at $\hbar\omega_{\text{tunable}} = \hbar\omega_{\text{SFG}} - \hbar\omega_{1064} = 1.7$ eV because no particular two-photon resonance was observed at ~2.85 eV in the corresponding SHG spectrum in Fig. 5(c). The same resonances were also detected from other vicinal surfaces of TiO_2 (6 7 1) and (17 18 1) in our recent work.[33] According to Ref. 33, the SHG/SFG enhancement at 2.6 eV is assigned to the resonance at a Ti defect state induced by oxygen vacancies or titanium interstitials, or a shallow electron trap (SET) state, whereas the enhancement at ~1.7 eV is assigned to the resonance at a localized O state, or a deep hole trap (DHT) state. The energy levels of these trap states are drawn in Fig. 7(a). In the SHG/SFG spectra of TiO_2 (110), in contrast, no significant resonance from a trap state was detected below 3 eV as seen in Figs. 5(c) and 5(d). It follows that the step bunches play an important role in forming trap states.

In the DFT calculation, gap states similar to the DHT level were found only in the vicinity of the step edge (*S*-O3 and

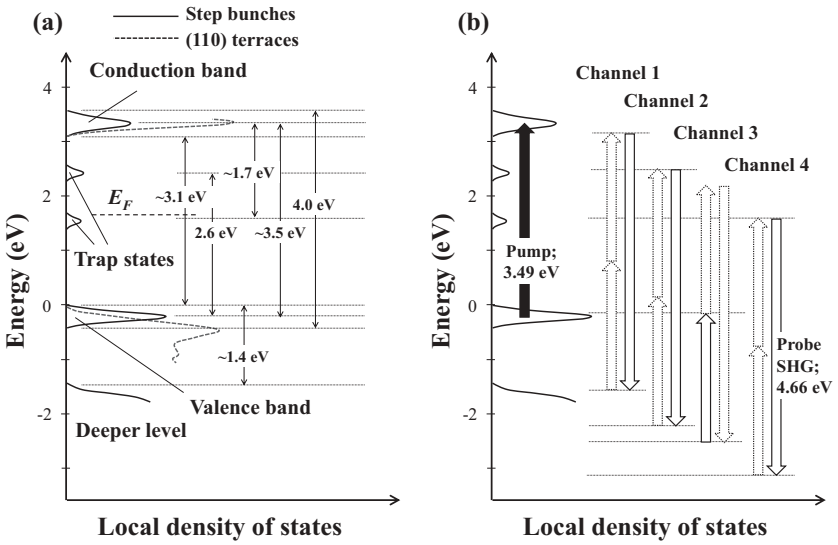

FIG. 7. (a) Schematic view of the LDOS distribution of the step bunches and (110) terraces on annealed TiO_2 (15 15 4) predicted from the SHG/SFG spectroscopy with the help of the DFT calculation. (b) Possible transition channels of probe SHG at the SHG photon energy of 4.66 eV in the time-resolved pump-probe SHG measurement. The energy zero at the vertical axis is set at the valence band maximum. Empty block arrows with dotted lines in (b) represent nonresonant SHG processes, and those with solid lines indicate resonant SHG processes.

S-O4). This result suggests that a step oxygen atom can be an important hole trapping site, whereas most hole trapping sites have been associated with oxygen atoms on a flat (110) surface.[55–62]

In summary, the SHG/SFG spectroscopy and the DFT calculation showed that the step bunches have clearly different electronic properties from the (110) terraces. The step bunches are rich in trap states such as SET and DHT states, and the valence band LDOS of the step bunches is blue shifted with respect to that of the (110) terraces.

C. Local carrier dynamics at the step bunches on annealed TiO_2 (15 15 4)

In this section we show the result of the time-resolved pump-probe SHG measurement combined with the step-selective SHG scheme and demonstrate the first selective observation of local dynamics at the step bunches on annealed TiO_2 (15 15 4). The SHG time profiles of annealed TiO_2 (15 15 4) for different pump fluences are shown in Figs. 8(a) and 8(c), and those of unannealed TiO_2 (15 15 4) are shown in Figs. 8(b) and 8(d). The SHG intensity in the vertical axis is normalized by the average SHG intensity at the negative time delay.

All of the time-resolved spectra in Fig. 8 display immediate changes in SHG intensity after the UV pump excitation (0 ps), and then long-lasting plateaus. For S in–S out [Figs. 8(a) and 8(b)], changes in SHG intensity are completely opposite between the annealed and unannealed samples. That is, the annealed sample displays the increase in SHG intensity with respect to the unmodulated SHG intensity during almost all the delay times, while the unannealed sample shows the decrease in SHG intensity. In contrast, both of the samples exhibit similar SHG intensity drops for P in–all out [Figs. 8(c) and 8(d)]. Note that the scale of the vertical axis in Fig. 8(a) is different from the others. Based on the same logic as in the previous section, the signal difference between the annealed and unannealed samples in Figs. 8(a) and 8(b) should be attributed to the different surface structures with different electronic properties, and hence the higher order bulk effects are negligible in these spectra. Furthermore, since the higher order bulk effect from TiO_2 (110) has been reported to be small enough at the 45 deg incidence,[63] the ones in Fig. 8 are not expected to be significant either.

The time profiles of annealed TiO_2 (15 15 4) measured for S in–S out [Fig. 8(a)] are relevant to χ^0_{xxx}, where χ^0_{ijk} is a χ element in the $\{x_0, y_0, z_0\}$ coordinate system (Fig. 4), and selectively reflect local dynamics at the step bunches (see the Appendix for details). The other time profiles in Figs. 8(b)–8(d) originate from the entire surfaces. For P in–all out in Fig. 8(c), the majority of the SHG modulations (approximately 80%) should be attributed to the (110) terrace contribution, as suggested from the SHG intensity ratio between (15 15 4) and (110) at 4.66 eV shown in Fig. S2(a) (see Supplemental Material[51]). As for unannealed TiO_2 (15 15 4), the SHG signals probed at S in–S out [Fig. 8(b)] originate from the broken symmetry in the horizontal direction (x direction) on the surface, while those probed at P in–all out [Fig. 8(d)] primarily originate from the broken symmetry in the vertical direction (z direction). The former case is generally more sensitive to the fine structure of the unannealed surface.

Only for 800 μJ/cm^2 in Fig. 8(a), an interesting sharp spike decaying within 100 ps was observed at the time delay of ~0 ps, while no decay kinetics was observed for other time profiles within 1 ns [Figs. 8(b)–8(d)]. This result strongly indicates that the decay kinetics of the step bunches is completely different from that of the other surface structures like the (110) terraces and the unreconstructed (15 15 4) surface. It seems that some interesting phenomena intrinsic to the step bunches are present on the annealed surface within 100 ps after the pump irradiation.

There are four candidate origins of the sharp spike in Fig. 8(a) as well as the other temporal SHG responses: (1) modulation of Fresnel factors,[44,45,64,65] (2) pump-induced increase in surface temperature,[44,45] (3) creation of surface oxygen vacancies,[66,67] (4) changes in electron populations in surface states, and (5) electric-field-induced SHG (EFISHG). Origin 1 corresponds to a linear effect, origins 2–4 are associated with second order nonlinear effects, and origin 5 is a third order nonlinear effect. We evaluate these candidate origins individually as below.

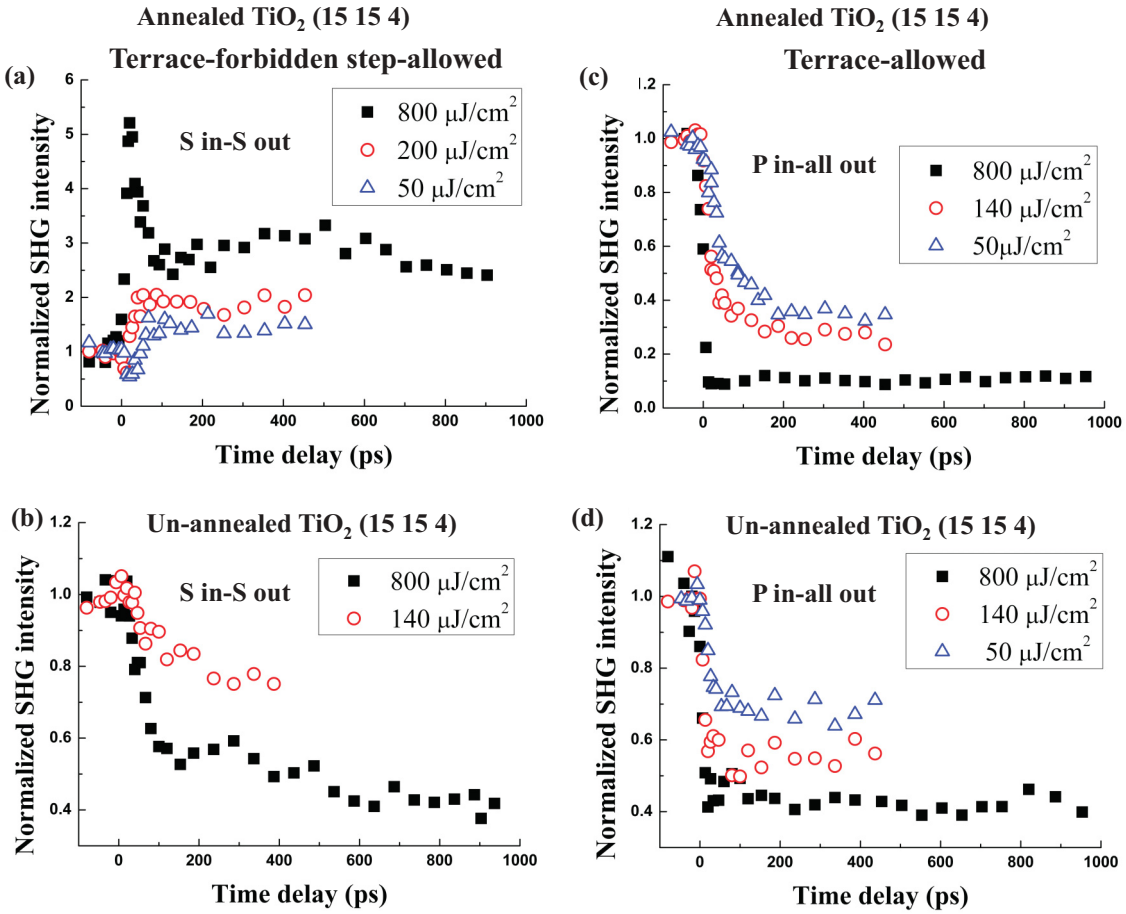

FIG. 8. (Color online) SHG intensity as a function of probe delay time with respect to the pump excitation for annealed and unannealed TiO_2 (15 15 4). (a) and (c) correspond to the annealed sample, and (b) and (d) correspond to the unannealed sample. The spectra in (a) and (b) were obtained at S in–S out, and those in (c) and (d) were obtained at P in–all out. The time-resolved pump-probe measurement was carried out at different fluences (50, 140, 200, and 800 $\mu J/cm^2$). The SHG intensity is normalized by the average intensity at the negative time delays.

First, let us discuss origin 1, modulation of Fresnel factors. The electric fields of SHG light emitted from the TiO_2 surfaces are modulated by Fresnel factors as follows:[44,45,64]

$$\mathbf{E}(2\omega) \propto F(2\omega) \cdot \chi^{(2)} : \{f(\omega) \cdot \mathbf{E}(\omega)\}\{f(\omega) \cdot \mathbf{E}(\omega)\}, \quad (1)$$

where $f(\omega)$ and $F(2\omega)$ are Fresnel factors at fundamental and doubled frequencies, respectively. Here one may think that the observed temporal SHG responses in Fig. 8 derive from the modulation of linear refractive indices included in the Fresnel factors. In order to estimate this linear effect, we carried out a time-resolved linear reflectivity measurement using the same optics as in Fig. 2. Since no reflectivity change was observed after the UV pump excitation, the linear effect including a local field factor can be neglected, and the observed time profiles in Fig. 8 should result from a nonlinear effect.

Second, we evaluate origin 2, pump-induced increase in surface temperature. Since $\chi^{(2)}$ is generally a function of temperature, an increase in surface temperature could give rise to a spikelike temporal SHG response as was seen for 800 $\mu J/cm^2$ in Fig. 8(a). As a matter of fact, a similar spike driven by a temperature jump was observed within several hundred picoseconds in time-resolved vibrational SFG spectra by Domen *et al.*.[39] As far as the SHG time profiles in Figs. 8(b)–8(d) are concerned, the effect of the temperature rise is excluded because no decay was observed even after a nanosecond. If the spikelike temporal SHG response in Fig. 8(a) is attributed to the temperature jump at the step bunches, then we need to interpret that the temperature goes up nonuniformly only at the step bunches on annealed TiO_2 (15 15 4) since the temperature on the (110) terraces does not rise at all as indicated in Fig. 8(c). Such a spatially nonuniform increase in surface temperature is not realistic. Therefore, the temperature jump is not the case here.

Additionally, origin 5 of EFISHG is not expected to contribute to the SHG modulations in Fig. 8. In general, it is induced by a charged region distributed across bulk or a near surface. However, our samples are neither reduced nor doped at all, and thus do not accumulate charges in the depth direction like an *n*- or *p*-type semiconductor. Moreover, if EFISHG were the case, both of the annealed and unannealed samples should have shown similar SHG responses since EFISHG is more like a bulk-originated response.

Most of the behaviors in Fig. 8 can be explained from the standpoint of origin 3 (creation of surface oxygen vacancies) and/or origin 4 (changes in electron populations in surface states). We first focus on the dynamics at the (110) terraces on annealed TiO_2 (15 15 4) [Fig. 8(c)] to interpret the dynamics at the step bunches [Fig. 8(a)]. In Fig. 8(c) the SHG intensity

drops seen for lower fluences can be divided into two steps: The initial sharp drops within the pump pulse duration (step 1) and the relatively slow drops lasting until ~200 ps (step 2). Step 1 can be interpreted as direct desorption of surface lattice oxygen atoms by the UV pump pulse (origin 3) and/or electron population changes in surface states by the carriers directly excited at the (110) terraces (origin 4). Step 2 is linked to the photoexcited electrons and holes reaching the surface afterwards through random migration from the bulk to the surface. More specifically, it can be ascribed to surface oxygen vacancy creation by some of these diffusing holes (origin 3) as[68]

$$2h^+ + O^{2-}_{\text{lattice}} \rightarrow 1/2\ O_2(g) + \text{oxygen vacancy}, \qquad (2)$$

and/or population changes in surface electronic states through the carrier migration from bulk (origin 4). As seen in the spectrum for 800 μJ/cm^2 in Fig. 8(c), when the pump fluence gets high enough, the effect of step 2 should become nearly invisible due to the high enough concentration of surface oxygen vacancies or photoexcited electrons and holes generated during step 1.

Let us check specific length and time scales associated with a carrier diffusion process like step 2. Generally speaking, diffusion forces from a surface to bulk are applied to excited carriers due to the concentration gradient generated by photoexcitation. Based on Fick's first law, initial diffusion velocity of excited carriers at the surface is roughly estimated to be $v = D/l \cong 400$ cm/s, or 0.04 nm per 10 ps. Here D is the diffusion coefficient of carriers, 1.34×10^{-2} cm^2/s,[69] and l is the penetration depth for the 355 nm pump light, ~330 nm.[70] Since this slow diffusion velocity becomes even smaller as time passes by, the diffusion from the surface to the bulk due to the concentration gradient is not significant during the time scale of this experiment. Thus excited carriers are assumed to be just randomly diffusing without changing their spatial distribution and then contribute to step 2. However, only a limited amount of excited carriers near the surface can contribute to step 2 because the diffusion length of carriers within 200 ps is estimated to be $L = \sqrt{Dt} \cong 16$ nm.

As far as the sharp spike in Fig. 8(a) is concerned, origin 3 (creation of surface oxygen vacancies) can be ruled out because the decay time of the spike is too short (<100 ps) for oxygen molecules to heal the vacancies, considering that the reported time ranges of interfacial charge transfer to molecular oxygen are longer than the order of a microsecond.[71,72] It follows that the spike in Fig. 8(a) is correlated with some behavior of photoexcited carriers at the step bunches rather than the creation of surface oxygen vacancies there, and thus is attributed to origin 4. Moreover, since the initial rise of the spike completes within the pulse duration, direct excitation at the step bunches (step 1) should be mainly responsible for the spikelike temporal response. According to our simple estimation of diffusion length, excited carriers at the depth of less than ~6 nm may also contribute to the temporal response to some extent through carrier migration (step 2).

If we assume the band structure of the step bunches suggested in the previous section [Fig. 7(a)], four possible transition channels of probe SHG is considered to contribute to the SHG temporal responses at the spike, as illustrated in Fig. 7(b). Channels 1 and 2 correspond to transitions from the deeper level below the valence band to the conduction band and to the SET states, respectively. Channels 3 and 4 are pump-induced transition paths from the deeper level to the valence band and to the DHT states, respectively, and are not active for an unexcited surface because the two real electronic states relevant to SHG transitions are filled. Upon the photoexcitation by the UV pump pulse, cooling[73,74] and trapping[1,75,76] processes of photoexcited electrons and holes are expected to complete within 1 ps. After these relaxation processes, the SET states and the electronic states near the CBM transiently become occupied, while the DHT states and the electronic states near the VBM become unoccupied states. Resultantly, the SHG processes through channels 1 and 2 are suppressed immediately after the UV pulse excitation, whereas the photoexcitation opens up channels 3 and 4. Channel 1 may be the main contribution in the SHG signal before pumping, but once the surface is pumped, all four channels with different phases can modify SHG. The spike temporal response in Fig. 8(a) is caused by the interplay of these channels and is presumably correlated with surge in local carrier density at the step bunches upon the photoexcitation and the following decay through carrier recombination or diffusion.

The significant increase in local carrier density at the step bunches mentioned above may occur in the following way. As discussed in the previous section, the notable electronic properties of the step bunches are the richness in the trap states (SET and DHT states) and the blue shift of the valence band LDOS of the step bunches with respect to that of the (110) terraces [Fig. 7(a)]. The trap states abundant at the step bunches can capture nearby excited carriers within 1 ps,[1,75,76] and this can increase local carrier density at the step bunches more remarkably than on the (110) terraces. In addition, after the cooling process by phonon relaxation (<~1 ps),[73,74] photoexcited holes may fill the valence band of the step bunches more favorably than that of the (110) terraces. These features can be the factors to raise the local carrier density more significantly at the step bunches within the pulse duration of ~30 ps than on the (110) terraces. Such increase in local carrier density can modulate SHG transition channels 2, 3, and/or 4 in Fig. 7(b), and may result in the rapid increases in SHG intensity as is seen in Fig. 8(a).

Excess electrons and/or holes at the step bunches beyond some threshold density are expected to diminish through electron-hole recombination, three-carrier Auger recombination, trap-assisted recombination, or carrier diffusion to bulk, as seen in the decay in the spike [Fig. 8(a)]. In general, the rates of bulk electron-hole recombination and three-carrier Auger recombination are very slow for TiO_2. For instance, the half-time of electron-hole recombination decay in single crystal rutile TiO_2 is estimated to be $\tau = 1/kN_0 \approx 50$ ns, where k is an electron-hole recombination rate constant (=5×10^{-13} cm^3/s),[77] and N_0 is initial surface carrier density before relaxation estimated for the fluence of 800 μJ/cm^2 (≈4×10^{19} cm^{-3}). If the two-carrier or three-carrier recombination is to contribute to the decay within ~100 ps, initial local carrier density of more than 1×10^{22} cm^{-3} is required at the step bunches for the former, and more than 1×10^{21} cm^{-3} is required for the latter, under assumption of $k = 5 \times 10^{-13}$ cm^3/s (Ref. 77) and Auger recombination coefficient of $\gamma = 1 \times 10^{-32}$ cm^6/s.[78] These values are nearly

two or three orders of magnitude larger than the above N_0 value, and thus these two recombination paths may not be predominant. Therefore, the decay through the trap-assisted recombination or the carrier diffusion is more likely to happen at the step bunches. Note that the interfacial charge transfer to reacting molecules such as H_2O and O_2 is reported to occur above the order of a microsecond[1,71,72,79] and hence does not contribute to the decay in Fig. 8(a). Absence of spikes for relatively low pump fluences in Fig. 8(a) is probably because the local carrier density at the step bunches is below the threshold of these decay processes. We believe that Coulomb carrier-carrier interaction is not directly relevant to the decay because it is generally significant within the order of a hundred femtoseconds.[80]

In this manner we have selectively observed fast local carrier dynamics unique to the step bunches on annealed TiO_2 (15 15 4) by utilizing the step-selective property of SHG. We stress that this sort of a selective probe to zoom up local carrier dynamics at active sites like steps can open up a new window to reveal a photocatalytic reaction mechanism.

IV. CONCLUSION

In this study we demonstrated the selective observation of local carrier dynamics at the step bunches on annealed vicinal TiO_2 (110) or (15 15 4) by incorporating the step-selective SHG property into the time-resolved pump-probe SHG method. The time-resolved SHG spectra of the step bunches displayed a unique temporal response such as a sharp spike decaying within ~100 ps at the high fluence of 800 $\mu J/cm^2$, while no decay kinetics was observed for the (110) terraces within a nanosecond. The spike was attributed to a transient change in local carrier density at the step bunches. We conducted the LDOS analysis by the SHG/SFG spectroscopy and the DFT calculation, and it was found that the step bunches are rich in trap states such as SET and DHT states, and that the valence band LDOS distribution of the step bunches is blue shifted with respect to that of the (110) terraces. We suggest that these characteristic local electronic states can be responsible for the unique temporal behaviors of SHG from the step bunches.

ACKNOWLEDGMENTS

This work was supported by Grant-in-Aid for Scientific Research (c) (23540363) of Japan Society for the Promotion of Science (JSPS). The authors would like to thank Dr. A. Steigerwald for helpful advices. The authors are grateful to Y. Nakabayashi and M. Uno for experimental support.

APPENDIX

In the Appendix we give a detailed discussion on the step selectivity of SHG for vicinal TiO_2 (110) by reviewing and reinforcing the discussion previously given in Ref. 34. Strictly speaking, the components of fundamental and reflected SHG electric fields perpendicular to the (110) terrace plane is not completely zero even in the step-selective configuration since the terrace plane of annealed TiO_2 (15 15 4) is tilted from the surface plane by 16.2 deg, and thus a certain amount of a terrace contribution produced by the vertical electric fields might be mixed into the SHG signal. Hence we estimated experimentally how much terrace contribution can be contained in the SHG signal under the step-selective optical configuration and verified if SHG is indeed suitable as a step-selective probe for vicinal TiO_2 (110). In the following discussion on the step-selective property of SHG, we focus only on the dipole surface SHG from annealed TiO_2 (15 15 4).

As shown in Fig. 4, we think of two orthogonal coordinate systems to separate the step and terrace contributions. One is the laboratory coordinate of $\{x, y, z\}$, and the other is the crystal coordinate of $\{x_0, y_0, z_0\}$, where $x = [\bar{2}\,\bar{2}\,15]$, $z = [15\,15\,4]$, $x_0 = [001]$, $z = [110]$, and $y = y_0 = [1\bar{1}0]$. The former coordinate system is defined by the rotation of the latter around the y_0 axis by the angle θ of 16.2 deg [referred to as the operation $F(\theta)$]. The position vectors between the two coordinate systems satisfy the relation $\mathbf{r}_0 = F(\theta)\cdot\mathbf{r}$. Now we think of two second order nonlinear susceptibility elements directly relevant to the SHG intensity measured in the step-selective configuration: χ_{xyy} and χ_{xxx}, where χ_{ijk} is a second order nonlinear susceptibility element in the $\{x, y, z\}$ coordinate system. These two susceptibility elements can be expressed by the ones in the $\{x_0, y_0, z_0\}$ coordinate system as follows:

$$\chi_{xyy} = \sum_{ijk} F_{xi}(\theta)\chi^0_{ijk}F_{jy}(-\theta)F_{ky}(-\theta)$$
$$= \left(\chi^0_{xyy} - \chi^0_{zyy}\tan\theta\right)\cos\theta, \quad \text{(A1)}$$

$$\chi_{xxx} = \sum_{ijk} F_{xi}(\theta)\chi^0_{ijk}F_{jx}(-\theta)F_{kx}(-\theta)$$
$$= \left\{\chi^0_{xxx} - \left(2\chi^0_{xxz} + \chi^0_{zxx}\right)\tan\theta + \left(2\chi^0_{zxz} + \chi^0_{xzz}\right)\tan^2\theta - \chi^0_{zzz}\tan^3\theta\right\}\cos^3\theta. \quad \text{(A2)}$$

Here χ^0_{ijk} is a second order nonlinear susceptibility element in the $\{x_0, y_0, z_0\}$ coordinate system, and $F_{ij}(\theta)$ is an element of the transformation matrix $F(\theta)$. χ^0_{zyy}, χ^0_{xxz}, χ^0_{zxx}, and χ^0_{zzz} are associated with both steps and terraces, while χ^0_{xyy}, χ^0_{xxx}, χ^0_{zxz}, and χ^0_{xzz} stem from the pure step contribution and have finite values only in the vicinity of the step bunches. In order to realize the step-selective SHG measurement, the tanθ term in Eq. (A1) and the terms of tanθ and tan$^3\theta$ in Eq. (A2) must be much smaller than the first terms of χ^0_{xyy} and χ^0_{xxx}, respectively. However, we have to note that the contributions of χ^0_{zyy}, χ^0_{xxz}, and χ^0_{zxx} are smaller just by the factor of tanθ (=0.29) than those from χ^0_{xyy} and χ^0_{xxx}. Especially, the χ^0_{xxz} component in Eq. (A2) is reported to provide relatively high contribution to SHG for a (110) face.[63] Hence we particularly focus on Eq. (A2) and consider the relative size of each χ^0_{ijk} contribution in χ_{xxx} as below.

Our previous study of TiO_2 (15 15 4) suggests that the size of the step contribution in χ_{xxx} can be comparable with that of the terrace contribution or can be even larger depending on the photon energy range.[34] In Fig. S2(a) we cite the previous result from Ref. 34 (see Supplemental Material[51]). The vertical axis corresponds to the SHG intensity ratio of annealed TiO_2 (15 15 4) to TiO_2 (110) measured under the optical geometry

of ∼45 deg incidence, P in–P out, and x_0 azimuth (or x azimuth). In this optical configuration, relevant second order nonlinear susceptibility components for TiO_2 (15 15 4) are χ^0_{xxz}, χ^0_{zxx}, χ^0_{zzz}, χ^0_{xxx}, χ^0_{zxz}, and χ^0_{xzz}; and those for TiO_2 (110) are χ^0_{xxz}, χ^0_{zxx}, and χ^0_{zzz}. Since their difference χ^0_{xxx}, χ^0_{zxz}, and χ^0_{xzz} originate from the pure step contribution, the deviation from unity in Fig. S2(a) is almost the direct measure of the step contribution. The significant deviation around 3.5 eV clearly shows that the step contribution is even larger than the terrace contribution near this photon energy. Thus χ_{xxx} is nearly equivalent to χ^0_{xxx} around the photon energy of 3.5 eV.

It is also important to note that the SHG intensity ratio in Fig. S2(a) is nearly unity at the photon energies between 4.1 and 4.4 eV. This result suggests that the pure step contribution of χ^0_{xxx}, χ^0_{zxz}, and χ^0_{xzz} is very small in this photon energy range. Accordingly, the SHG signals given by χ_{xxx} should mostly derive from the terrace contribution of χ^0_{xxz}, χ^0_{zxx}, and χ^0_{zzz} in Eq. (A2) at the photon energies between 4.1 and 4.4 eV. Moreover, these three elements are reported to give nearly the maximum SHG intensity at the photon energies above ∼3.8 eV for TiO_2 (110).[63] Hence between 4.1 and 4.4 eV the χ_{xxx} element must exhibit the maximum possible SHG from the terraces, and the corresponding SHG intensity indicates the noise level of step-selective SHG. In Fig. 5(c) the χ_{xxx} element actually gives almost the minimum SHG intensity in the same photon energy range within the energy window between 2.3 and 4.7 eV. These experimental facts suggest that the absolute amount of the terrace contribution contained in χ_{xxx} [Eq. (A2)] is very small in the whole photon energy range of interest. Additionally, the terrace contribution of χ^0_{zyy} in χ_{xyy} [Eq. (A1)] is also expected to be negligible since the contribution of χ^0_{zyy} is even smaller than that of χ^0_{xxz} as reported by Omote *et al.*.[63]

For the more quantitative investigation of the step contribution in χ_{xxx}, we examined polarization angle dependence of SHG intensity for annealed TiO_2 (15 15 4) at the grazing incidence. In this SHG measurement the same optics as was used for the SHG spectroscopy [Fig. 1(a)] was employed, except for the incident angle. The incident angle was fixed at ∼85 deg, and the photon energy of the observed SHG beam was tuned at 3.65, 3.88, 4.13, and 4.66 eV. The incident plane was set parallel to $[1\bar{1}0]$. In this experiment, SHG intensity was compared between two types of polarization geometries, namely, S in–S out and S + 16.2° in–S + 16.2° out. Here S + 16.2° denotes the polarization of the electric field rotated by 16.2 deg from S polarization in the direction such that the electric field becomes parallel to the (110) terrace plane of annealed TiO_2 (15 15 4). By comparing these two cases, one can get an idea about the accuracy of the step selectivity under the proposed optical geometry. The result is shown in Fig. S2(b) (see Supplemental Material[51]). In this graph SHG intensity for S + 16.2° in–S + 16.2° out ($=I_{S+16.2}$) is divided by that for S in–S out ($=I_S$), and thus the vertical axis represents $|\chi^0_{xxx}/\chi_{xxx}|^2 = I_{S+16.2}/I_S$. Deviation from unity in the vertical axis implies the terrace contribution. The deviation is large at 4.13 eV in Fig. S2(b) because the step contribution becomes very small and comparable to the terrace one at the photon energies between 4.1 and 4.4 eV as discussed above. At the other photon energies of 3.65, 3.88, and 4.66, the differences between $I_{S+16.2}$ and I_S were found to be less than 10%, and thus the step contribution is dominant in χ_{xxx}.

Taking all the above experimental facts into account, high enough step selectivity of the surface SHG from χ_{xxx} and χ_{xyy} is guaranteed near the main resonant energies of ∼3.5 and ∼4.6 eV as long as the electric fields of fundamental and reflected SHG/SFG light are set nearly parallel to the *surface plane* of annealed TiO_2 (15 15 4).

*Corresponding author: mizutani@jaist.ac.jp

[1] A. Fujishima, X. Zhang, and D. A. Tryk, Surf. Sci. Rep. **63**, 515 (2008).

[2] U. Diebold, Surf. Sci. Rep. **48**, 53 (2003).

[3] A. Fujishima, T. N. Rao, and D. A. Tryk, J. Photochem. Photobiol. C: Photochem. Rev. **1**, 1 (2000).

[4] A. Fujishima and K. Honda, Bull. Chem. Soc. Jpn. **44**, 1148 (1971).

[5] A. Fujishima and K. Honda, Nature (London) **238**, 37 (1972).

[6] X.-Q. Gong and A. Selloni, J. Catal. **249**, 134 (2007).

[7] X.-Q. Gong, A. Selloni, M. Batzill, and U. Diebold, Nat. Mater. **5**, 665 (2006).

[8] X.-Q. Gong, A. Selloni, O. Dulub, P. Jacobson, and U. Diebold, J. Am. Chem. Soc. **130**, 370 (2008).

[9] A. Sasahara, C. L. Pang, and H. Onishi, J. Phys. Chem. B **110**, 4751 (2006).

[10] S. Suzuki, Y. Yamaguchi, H. Onishi, K. Fukui, T. Sasaki, and Y. Iwasawa, Catal. Lett. **50**, 117 (1998).

[11] Y. Iwasawa, H. Onishi, and K. Fukui, Top. Catal. **14**, 163 (2001).

[12] Y. Du, Z. Dohnálek, and I. Lyubinetsky, J. Phys. Chem. C **112**, 2649 (2008).

[13] S. Wendt, R. Schaub, J. Matthiesen, E. K. Vestergaard, E. Wahlström, M. D. Rasmussen, P. Thostrup, L. M. Molina, E. Lægsgaard, I. Stensgaard, B. Hammer, and F. Besenbacher, Surf. Sci. **598**, 226 (2005).

[14] E. Lira, J. Ø. Hansen, P. Huo, R. Bechstein, P. Galliker, E. Lægsgaard, B. Hammer, S. Wendt, and F. Besenbacher, Surf. Sci. **604**, 1945 (2010).

[15] R. Schaub, P. Thostrup, N. Lopez, E. Lægsgaard, I. Stensgaard, J. K. Norskov, and F. Besenbacher, Phys. Rev. Lett. **87**, 266104 (2001).

[16] S. Wendt, J. Matthiesen, R. Schaub, E. K. Vestergaard, E. Lægsgaard, F. Besenbacher, and B. Hammer, Phys. Rev. Lett. **96**, 066107 (2006).

[17] I. M. Brookes, C. A. Muryn, and G. Thornton, Phys. Rev. Lett. **87**, 266103 (2001).

[18] C. Di Valentin, G. Pacchioni, and A. Selloni, Phys. Rev. Lett. **97**, 166803 (2006).

[19] C. M. Yim, C. L. Pang, and G. Thornton, Phys. Rev. Lett. **104**, 036806 (2010).

[20] F. M. Hossain, G. E. Muech, L. Sheppard, and J. Nowotny, Solid State Ionics **178**, 319 (2007).

[21] S. Munnix and M. Schmeits, Phys. Rev. B **31**, 3369 (1985).
[22] M. Tsukada, H. Adachi, and C. Satoko, Prog. Surf. Sci. **14**, 113 (1983).
[23] M. A. Henderson, W. S. Epling, C. L. Perkins, and C. H. F. Peden, J. Phys. Chem. B **103**, 5328 (1999).
[24] M. A. Henderson, W. S. Epling, C. H. F. Peden, and C. L. Perkins, J. Phys. Chem. B **107**, 534 (2003).
[25] S. Wendt, P. T. Sprunger, E. Lira, G. K. H. Madsen, Z. Li, J. Ø. Hansen, J. Matthiesen, A. Blekinge-Rasmussen, E. Lægsgaard, B. Hammer, and F. Besenbacher, Science **320**, 1755 (2008).
[26] N. O. Gopal, H.-H. Lo, S.-C. Sheu, and S.-C. Ke, J. Am. Chem. Soc. **132**, 10982 (2010).
[27] Z. Zhang, J. Lee, J. T. Yates Jr., R. Bechstein, E. Lira, J. Ø. Hansen, S. Wendt, and F. Besenbacher, J. Phys. Chem. C **114**, 3059 (2010).
[28] C. W. van Hasselt, M. A. Verheijen, and Th. Rasing, Phys. Rev. B **42**, 9263 (1990).
[29] J. R. Power, J. D. O'Mahony, S. Chandola, and J. F. McGilp, Phys. Rev. Lett. **75**, 1138 (1995).
[30] P. Kratzer, E. Pehlke, M. Scheffler, M. B. Raschke, and U. Höfer, Phys. Rev. Lett. **81**, 5596 (1998).
[31] K. Stépán, M. Dürr, J. Güdde, and U. Höfer, Surf. Sci. **593**, 54 (2005).
[32] G. G. Malliaras, H. A. Wierenga, and Th. Rasing, Surf. Sci. **287-288**, 703 (1993).
[33] H. Takahashi, R. Watanabe, Y. Miyauchi, and G. Mizutani, J. Chem. Phys. **134**, 154704 (2011).
[34] H. Takahashi, R. Watanabe, and G. Mizutani, Surf. Interface Anal. **42**, 1659 (2010).
[35] H. Takahashi, R. Watanabe, and G. Mizutani, e-j. Surf. Sci. Nanotech. **8**, 84 (2010).
[36] S. Janz, D. J. Bottomley, H. M. van Driel, and R. S. Timsit, Phys. Rev. Lett. **66**, 1201 (1991).
[37] I. Yagi, M. Chiba, and K. Uosaki, J. Am. Chem. Soc. **127**, 12743 (2005).
[38] Y. Maeda, T. Iwai, Y. Satake, K. Fujii, S. Miyatake, D. Miyazaki, and G. Mizutani, Phys. Rev. B **78**, 075440 (2008).
[39] J. Chen, J. Kubota, A. Wada, J. N. Kondo, and K. Domen, J. Am. Chem. Soc. **131**, 4580 (2009).
[40] J. M. Lantz and R. M. Corn, J. Phys. Chem. **98**, 9387 (1994).
[41] D. Bodlaki and E. Borguet, Appl. Phys. Lett. **83**, 2357 (2003).
[42] Yu. D. Glinka, W. Wang, S. K. Singh, Z. Marka, S. N. Rashkeev, Y. Shirokaya, R. Albridge, S. T. Pantelides, N. H. Tolk, and G. Lucovsky, Phys. Rev. B **65**, 193103 (2002).
[43] Y. D. Glinka, N. H. Tolk, X. Liu, Y. Sasaki, and J. K. Furdyna, Phys. Rev. B **77**, 113310 (2008).
[44] C. Guo, G. Rodriguez, and A. J. Taylor, Phys. Rev. Lett. **86**, 1638 (2001).
[45] J. Hohlfeld, U. Conrad, and E. Matthias, Appl. Phys. B **63**, 541 (1996).
[46] Y. M. Chang, L. Xu, and H. W. K. Tom, Phys. Rev. Lett. **78**, 4649 (1997).
[47] H. B. Zhao, Y. Fan, G. Lüpke, A. T. Hanbicki, C. H. Li, and B. T. Jonker, Phys. Rev. B **83**, 212302 (2011).
[48] W. A. Tisdale, K. J. Williams, B. A. Timp, D. J. Norris, E. S. Aydil, and X.-Y. Zhu, Science **328**, 1543 (2010).
[49] J. P. Perdew, K. Burke, and M. Ernzerhof, Phys. Rev. Lett. **77**, 3865 (1996).
[50] S. J. Clark, M. D. Segal, C. J. Packard, P. J. Hasnip, M. I. J. Probert, K. Refson, and M. C. Payne, Z. Kristallogr. **220**, 567 (2005).
[51] See Supplemental Material at http://link.aps.org/supplemental/10.1103/PhysRevB.86.045447 for experimental and theoretical analysis of second order nonlinear susceptibility of TiO_2 (15 15 4) by rotational SHG measurement (Fig. S1), and SHG analysis of the relative size of the step contribution included in the SHG signal from annealed TiO_2 (15 15 4) (Fig. S2).
[52] A. V. Melnikov, A. A. Nikulin, and O. A. Aktsipetrov, Phys. Rev. B **67**, 134104 (2003).
[53] E. M. Kim, S. S. Elovikov, T. V. Murzina, A. A. Nikulin, O. A. Aktsipetrov, M. A. Bader, and G. Marowsky, Phys. Rev. Lett. **95**, 227402 (2005).
[54] E. D. Mishina, A. A. Fedyani, D. Klimkin, A. A. Nikulin, O. A. Aktsipetrov, S. L. Vorob'eva, V. R. Novak, M. A. C. Devillers, and Th. Rasing, Surf. Sci. **382**, L696 (1997).
[55] K. Ishibashi, A. Fujishima, T. Watanabe, and K. Hashimoto, J. Photochem. Photobiol. A: Chem. **134**, 139 (2000).
[56] T. Tachikawa, S. Tojo, M. Fujitsuka, and T. Majima, J. Phys. Chem. B **108**, 5859 (2004).
[57] Y. Nosaka, S. Komori, K. Yawata, T. Hirakawa, and A. Y. Nosaka, Phys. Chem. Chem. Phys. **5**, 4731 (2003).
[58] R. F. Howe and M. Grätzel, J. Phys. Chem. **91**, 3906 (1987).
[59] C. P. Kumar, N. O. Gopal, T. C. Wang, M.-S. Wong, and S. C. Ke, J. Phys. Chem. B **110**, 5223 (2006).
[60] N. O. Gopal, H.-H. Lo, S.-C. Sheu, and S.-C. Ke, J. Am. Chem. Soc. **132**, 10982 (2010).
[61] O. I. Micic, Y. Zhang, K. R. Cromack, A. D. Trifunac, and M. C. Thurnauer, J. Phys. Chem. **97**, 13284 (1993).
[62] O. I. Micic, Y. Zhang, K. R. Cromack, A. D. Trifunac, and M. C. Thurnauer, J. Phys. Chem. **97**, 7277 (1993).
[63] M. Omote, H. Kitaoka, E. Kobayashi, O. Suzuki, K. Aratake, H. Sano, G. Mizutani, W. Wolf, and R. Podloucky, J. Phys.: Condens. Matter **17**, S175 (2005).
[64] J. E. Sipe, D. J. Moss, and H. M. van Driel, Phys. Rev. B **35**, 1129 (1987).
[65] H. Sano, M. Kume, H. Nakagawa, and G. Mizutani, J. Appl. Phys. **91**, 4229 (2002).
[66] A. N. Shultz, W. Jang, W. M. Hetherington III, D. R. Baer, L.-Q. Wang, and J. H. Engelhard, Surf. Sci. **339**, 114 (1995).
[67] E. Kobayashi, K. Matsuda, G. Mizutani, and S. Ushioda, Surf. Sci. **427**, 294 (1999).
[68] S. H. Szczepankiewicz, A. J. Colussi, and M. R. Hoffmann, J. Phys. Chem. B **104**, 9842 (2000).
[69] S. Nakabayashi, S. Komuro, Y. Aoyagi, and A. Kira, J. Phys. Chem. **91**, 1696 (1987).
[70] G. E. Jellison Jr., F. A. Modine, and L. A. Boatner, Opt. Lett. **22**, 1808 (1997).
[71] A. Yamakata, T. Ishibashi, and H. Onishi, J. Phys. Chem. B **105**, 7258 (2001).
[72] T. Yoshihara, R. Katoh, A. Furube, Y. Tamaki, M. Murai, K. Hara, S. Murata, H. Arakawa, and M. Tachiya, J. Phys. Chem. B **108**, 3817 (2004).
[73] E. Hendry, F. Wang, J. Shan, T. F. Heinz, and M. Bonn, Phys. Rev. B **69**, 081101(R) (2004).
[74] O. V. Prezhdo, W. R. Duncan, and V. V. Prezhdo, Prog. Surf. Sci. **84**, 30 (2009).
[75] Y. Tamaki, K. Hara, R. Katoh, M. Tachiya, and A. Furube, J. Phys. Chem. C **113**, 11741 (2009).
[76] K. Iwata, T. Takaya, H. Hamaguchi, A. Yamakata, T. Ishibashi, H. Onishi, and H. Kuroda, Chem. B **108**, 20233 (2004).

[77]R. Katoh, M. Murai, and A. Furube, Chem. Phys. Lett. **461**, 238 (2008).

[78]Y. Yamada and Y. Kanemitsu, Phys. Rev. B **82**, 113103 (2010).

[79]Y. Tamaki, A. Furube, M. Murai, K. Hara, R. Katoh, and M. Tachiya, J. Am. Chem. Soc. **128**, 416 (2006).

[80]R. Binder, D. Scott, A. E. Paul, M. Lindberg, K. Henneberger, and S. W. Koch, Phys. Rev. B **45**, 1107 (1992).